# Metabolomic profiling during the differentiation of human induced pluripotent stem cells into hepatocyte-like cells

Rachid Jellali, Myriam Lereau Bernier, Yannick Tauran, Françoise Gilard, Mathieu Danoy, Taketomo Kido, Atsushi Miyajima, Yasuyuki Sakai, Eric Leclerc

# Metabolomic profiling during the differentiation of human induced pluripotent stem cells into hepatocytes like cells

Jellali Rachid[1+], Myriam Lereau Bernier[2+], Yannick Tauran[2,3], Françoise Gilard[4], Mathieu Danoy[2], Taketomo Kido[5], Atsushi Miyajima[5], Yasuyuki Sakai[6], Eric Leclerc[2*]

[1] *CNRS UMI 7338, Laboratoire de Biomécanique et Bioingénierie, Sorbonne universités, Université de Technologies de Compiègne, France*

[2] *CNRS UMI 2820; Laboratory for Integrated Micro Mechatronic Systems, Institute of Industrial Science, University of Tokyo; 4-6-1 Komaba; Meguro-ku; Tokyo 153-8505, Japan*

[3] *LMI CNRS UMR5615, Université Lyon 1, Villeurbanne, 69622, France*

[4] *Institute of Plant Sciences Paris-Saclay (IPS2), UMR 9213/UMR1403, CNRS, INRA, Université Paris-Sud, Université d'Evry, Université Paris-Diderot, Sorbonne Paris-Cité, Saclay Plant Sciences, Bâtiment 630, 91405 0rsay, France*

[5] *Laboratory of Stem Cell Therapy, Institute for Quantitative Biosciences, The University of Tokyo, 1-1-1 Yayoi, Bunkyo-ku, Tokyo 113-0032, Japan*

[6] *CIBIS; Institute of Industrial Science; The University of Tokyo; 4-6-1 Komaba; Meguro-ku; Tokyo 153-8505, Japan*

+ Authors with equal contribution

* corresponding author: Eric Leclerc: eleclerc@iis.u-tokyo.ac.jp

Rachid Jellali: rachid.jellali@utc.fr

**Abstract**

Human induced pluripotent stem cells (hiPSC) potentially present an invaluable source of cells for regenerative medicine, disease modeling and drug discovery. However, hiPSC differentiation into fully functional hepatocytes remains a major challenge. Despite the importance of information carried by metabolomes, the exploitation of metabolomics for characterizing and understanding of hiPSC differentiation remains largely unexplored. Here, to increase the knowledge on hiPSC maturation into mature hepatocytes, we investigated their metabolomics profiles during a sequential step-by-step differentiation: definitive endoderm (step 1), specification into hepatocytes (step 2), progenitor hepatocytes (step 3) and mature hepatocyte-like cells (step 4). Metabolomics biomarkers illustrated a switch from glycolysis-based respiration in step 1 to an oxidative phosphorylation in step 4. The step 1 was characterised by fatty acids beta oxidation, sorbitol metabolism and pentose phosphate pathway, glutamine and glucose metabolisms as potential various energy source. Complex lipid metabolism switch was monitored via the reduction of lipid production from steps 1 to 4, whereas high glycerol production occurred mainly step 4. The nitrogen cycle, *via* the urea production also was typical mechanism revealed in step 4. Our analysis may contribute to a better understanding of differentiation and suggest novel targets to improve iPSC maturation into functional hepatocytes.

**Keywords:** Metabolomics; induced pluripotent stem cells; hepatocyte; differentiation

## Introduction

During drug development, the strong contribution of chemical reactive metabolites, in Drug-Induced Liver Injury (DILI), including idiosyncratic hepatotoxicity, is acknowledged by scientific community, but still cannot be detected by conventional animal toxicity studies. Several compounds have progressed into human trials and have then caused severe hepatotoxicity, and no patterns existed in the animal studies that signaled these events (due to interspecies differences in bioavailability, the short life time of toxic adducts, the distribution and metabolism also explain a number of false positives and negatives, David et al., 2010; Sistare et al., 2016). About 1100 drugs compounds have been reported to induce DILI, which remains a leading cause of restrictions on use and withdrawal of drugs (Reuben et al., 2014; Kuna et al., 2018). Progress has been made in the development of tools to identify the risk for DILI. Nevertheless, the limited availability of human functional models for drug testing and relevant biomarkers identification remain a major bottleneck (Chen et al., 2014).

In 2007, Yamanaka's team achieved a major breakthrough by developing a technology for reprogramming patient somatic cells into human induced pluripotent stem cells (hiPSC, Takahashi et al., 2007). The availability of these cells with their ability to generate different cell types has tremendous potential in terms of study models in pharmaco-toxicology and cell therapy (such as patient derived investigation). It is currently assumed that human pluripotent stem cells can be differentiated into Hepatocytes Like Cells, HEP-LCs (Touboul et al, 2010, Hay et al., 2008, Cai et al, 2007). Those cells have the potential to reflect the adult human liver

and its development (and thus be used for biomarker discovery, Rashid et al, 2010, Holmgren et al., 2014). However, the achievement of fully functional hepatocytes cells is still challenging and they express a large heterogeneity (Godoy et al., 2015).

The metabolomics, or the study of the metabolome, consists of analyzing the compounds produced by chemical reactions taking place in cells or the whole organism. It makes it possible to identify variations in the culture medium or the cellular fluid composition and the metabolic changes (Nicholson et al., 1999). The biomarkers and the cellular signatures are then identified using statistics methods applied on the datasets (Sun et al., 2016, Nicholson et al., 1999). Data-driven approaches (data reduction *via* clustering, classification using for instance neural network, visualization using principal component analysis and then network analysis) make use of now-prevalent high throughput datasets that facilitate the elucidation of underlying biological mechanism. Knowledge-based approach relies on the increase use of systems biology to integrate heterogeneous data into existing knowledge-databases (Metabolite Set Enrichment Analysis MSEA, pathway network-KEGG, customized system biology model, etc…). Knowledge-based approach aims to facilitate the understanding of disease and biological process mechanisms (mechanistic analysis) at the systemic level (Sun et al, 2016; Mischak et al., 2010).

Several investigations of the metabolome are reported in the literature to characterize hepatic profiles and liver physiopathology (Safaei et al. 2016; Wruck et al., 2015). Furthermore, the hepatic metabolome is also changed along the liver development (Wu et al., 2018). In the present study, we have investigated the hiPSC metabolome during their differentiation into hepatocytes in order to understand the

evolution of the cellular metabolic profile during the iPSC *in vitro* maturation. We have integrated both data-driven and knowledge-based approaches to characterize the differentiation of hiPSC into hepatocyte like cells. The data driven approach lead to the signature identification during the step by step hiPSC differentiation. The knowledge-based approaches contribute to improve the analysis performance in identifying biomarkers and metabolic fates by highlighting the mechanistic and signaling pathways modulated during the step by step differentiation. The panel of signatures and of pathways, and their kinetics, during the differentiation is then discussed with literature *in vivo* and primary human *in vitro* datasets.

## 2. Materials and methods

### 2.1 Cell source

The hiPSC used in this study (TKDN4-M clones) were provided from the stem cell bank of the Institute of Medical Science of the University of Tokyo (established using a retrovirus harbouring four reprogramming factors, *OCT3/4*, *SOX2*, *KLF4*, and *c-MYC*). TkDN−4M hiPSC were cultivated following previously published protocols for cell differentiation (Si Tayeb et al., 2010).

### 2.2 hiPSCs differentiation protocol

Stem cells are cultivated on standard TCPS culture dish for initial expansion and all differentiation steps. Culture dishes (6 well plates) are coated with (20 mg/mL) Matrigel Matrix suited for iPS cells maintenance (Corning Matrigel hESC-Qualified

Matrix, ref. 354277) following manufacturer's instructions (incubation for 1h at 37°C). The exceeding amount of Matrigel is washed with DMEM before cell seeding. TkDN-4M cells are seeded at 10000 cells/$cm^2$. For maintenance and expansion, cells are cultivated in mTeSR 1 medium (StemCell Technologies, ref. 05850) complemented with the RHO/ROCK pathway inhibitor Y-27632 (StemCell Technologies, ref. 72302) for enhanced cells survival at thawing. After 24h and until the end of the expansion, the medium is renewed daily with pure mTeSR 1. During this initial process, the atmospheric condition is set at 37°C, 20% $O_2$, and 5% $CO_2$. The differentiation protocol is initiated when cell confluence reaches 90% (usually after 3 to 4 days).

The differentiation protocol consisted of four steps (here: step 1, step 2, step 3, and step 4; step 0 corresponding to the proliferation step) during which media compositions and atmospheric conditions are specifically defined. During the first step (step 1, 5 days, 37°C, 20% $O_2$, 5% $CO_2$), hiPS cells are cultivated in RPMI-1640 medium (Gibco) supplemented with B27 (Gibco) and Activin A (R&D Systems) at 100 ng/mL to achieve a definitive endoderm (DE) commitment. Then, as DE cells enters step 2 (5 days, 37°C, 5% $O_2$, 5% $CO_2$), they are cultivated in RPMI-1640 / B27 supplemented with FBF-2 (bFGF, Peprotech) at 10 ng/mL and BMP4 (Humanzyme) at 20 ng/mL (hepatic specification). At the end of step 2, cells commitment corresponds to hepatoblast progenitors. During step 3 (5 days, 37°C, 5% $O_2$, 5% $CO_2$), cells are cultivated in RPMI-1640 / B27 supplemented with HGF at 20 ng/mL to reach the hepatocytes progenitor commitment. In step 4 (S4, 37°C, 20% $O_2$, 5% $CO_2$), cells are cultivated in hepatocyte culture medium (Lonza HBM, ref. CC-3199 & CC-4182, without hEGF) supplemented with OSM (R&D Systems) at 20

ng/mL for 7 days to achieve mature hepatic cells. Culture medium is renewed every 24 hours.

## 2.3. Metabolomic analysis

### *2.3.1. Samples preparation and GC-MS analysis*

Samples preparation and metabolites extraction were performed according to our previous work (Jellali et al., 2018). 250 µL of culture medium (medium collected at the end of each step) were completed with 500 µL of frozen solution (-20°C) of water:acetonitrile:isopropanol (2:3:3) containing 4 mg/L of adonitol, 2.75 mg/L of α-aminobutyric acid solution (αABA), and placed in an eppendorf thermomixer for 10 min at 4°C with shaking at 1500 rpm. Insoluble material was removed by two centrifugations steps at 14000 rpm for 10 min. Three aliquots of each extract (200 µL) were dried for 4 h at 35 °C in a speed-vac and stored at -80°C until analysis.

All steps of GC-MS analyses were done as described in Fiehn et al. (2006; 2008). Samples were taken out of -80°C, warmed for 15 min and dried again for 1.5 h at 35 °C before adding 10 µL of 20 mg/mL methoxyamine in pyridine and the reaction was performed for 90 min at 30 °C with shaking. Then, 90 µL of N-methyl-N-trimethylsilyl-trifluoroacetamide (MSTFA, Regis Technologies) was added and the reaction continued for 30 min at 37 °C. After cooling, 100 µL was transferred to an Agilent vial for injection. Four hours after derivatization, 1 µL of sample was injected in splitless mode on an Agilent 7890B gas chromatograph coupled to an Agilent 5977A mass spectrometer. The column was an Rxi-5SilMS from Restek (30 m with

10 m Integra-Guard column - ref 13623-127). An injection in split mode with a ratio of 1:30 was systematically performed for saturated compound quantification. The oven temperature ramp was 60 °C for 1 min then 10 °C/min to 325 °C for 10 min. Helium constant flow was 1.1 mL/min. Temperatures were the following: injector: 250 °C, transfer line: 290 °C, source: 230 °C and quadrupole 150 °C. The quadrupole mass spectrometer was switched on after a 5.90 min solvent delay time, scanning from 50-600 u. Samples were randomized and fatty acid methyl ester mix (C8, C9, C10, C12, C14, C16, C18, C20, C22, C24, C26, C28, C30) was injected in the middle of the queue for external RI calibration.

Raw Agilent datafiles were analyzed with AMDIS (http://chemdata.nist.gov/mass- spc/amdis/). The Agilent Fiehn GC/MS Metabolomics RTL Library (version June 2008) was employed for metabolite identifications. Peak areas were determined with the Masshunter Quantitative Analysis (Agilent) in splitless and split 30 modes. Because automated peak integration was occasionally erroneous, integration was verified manually for each compound and peak areas were normalized to ribitol. Metabolite contents are expressed in arbitrary units (semi-quantitative determination).

*2.3.2. Statistical analyses and biomarker identification*

The metabolomic multivariate data analysis was performed with the XLSTAT.2016 software (Addinsoft) and MetaboAnalyst (Xia et al., 2012). Unsupervised Principal Component Analysis (PCA) and supervised Partial Least Squares-Discriminant Analysis (PLS-DA) were carried out in order to discover

significant variations between the groups. Discriminating metabolites were identified using the Variable Importance for the Projection (VIP) scores. Student's t-test was performed by prism 6.0 (GraphPad Software, San Diego). A *P* value less than 0.01 was considered statistically significant.

Metabolites with significant changes in the groups *(P* value < 0.01 and VIP > 1) were selected as biomarkers. Pathways analysis of potential biomarkers was performed with MetaboAnalyst (Xia et al., 2012).

**2.4 Glucose and lactate measurements**

Glucose consumption and lactate production were measured using an YSI 2950 Biochemistry Analyzer. For that purpose, 100 μL of culture medium were inserted in the analyser. Measurements are based on a direct reading of L-lactate (L-lactic acid) and glucose in culture medium by the YSI enzyme sensors, as the enzymes L-lactate oxidase and glucose oxidase are respectively immobilized in the lactate and glucose sensors.

**2.5 Albumin measurements**

To measure the production of albumin, we performed ELISA sandwich assays in a 96-well plate. The surface activation step was performed using anti-Human Albumin IgG (Bethyl, Japan) diluted at 1/1000 in a Tris buffer (0.1 M, pH = 8.0) overnight at 4°C. The passivation step was realized with gelatin (2 %) diluted in PBS and Tween 20 (0.1 %) and incubated for 1 hour. The samples were incubated 3h at

room temperature. After washing, the second anti-Human Albumin IgG coupled with peroxidase (Bethyl, Japan) was incubated at room temperature for 3h. The peroxidase activity was revealed by a mixture of $H_2O_2$ and OPD in citrate buffer (0.05 mM, pH = 7.4). The reaction was stopped with a sulfuric acid solution (4N) and the plate was read at 490nm (iMark Microplate reader, Bio-Rad).

### 2.6. Alpha fetoprotein measurements

To measure the production of alpha fetoprotein, we used the Abnova ELISA kit following the manufacturer's protocol (abnova KA0202 Alpha-Fetoprotein Human, ELISA Kit). Samples were diluted 1000 times for step 3 samples and 500 times for step 4 samples.

### 2.7. Immunostaining

After washing with phosphate buffer saline solution (PBS), cells were fixed in paraformaldehyde 4% at 4 °C overnight. Then, the cells were permeabilized with Triton X100 at 1/1000 for 15 min and washed with PBS. Fixed tissues were blocked in a solution (blocking buffer) for 30 min at room temperature (RT). Primary antibodies (CYP3A4 1/50,ALB 1/1000, AFP 1/1000, HNF4a 1/1000) were incubated overnight at 4 °C in blocking buffer. Secondary antibodies coupled with Alexa Fluor fluorochromes (Alexa 488, 647 and diluted at 1/500) were further in-cubated for 2 h at RT in the dark. Finally, DNA was stained with DAPI (342-07431, Dojindo) at 1/1000 for 15 min at RT in the dark. Observations were made with an Olympus IX-81 confocal laser-scanning microscope. The antibodies used were: CYP3A4 (rabbit,

ab135813, abcam), Albumin (goat, A80-129A, Bethyl), AFP (goat, sc-8109, Santa Cruz), HNF4a (Rabbit, ab181604, abcam) and Alexa Fluor 488 (donkey, ab150129, abcam).

## 3. Results

### 3.1. Hepatic stem cell lineage specification

At first, we confirmed the successful differentiation of the pluripotent stem cells toward liver like cells. The Figs 1A to 1D show the morphology at end of each differentiation step from step 1 to step 4. At the end of the differentiation process, in step 4, the cell tissue presented both monolayer areas and 3D aggregates. The monolayer area displayed typical hepatic cuboid shapes. The immunostaining confirmed the presence of HNF4a, albumin and CYP3A4 positive cells. However, the population was heterogeneous as far as all stained cells were not positive to albumin. In addition, the presence of AFP was detected (Figs. 1E to 1J). The functional assay confirmed a production of albumin equal to 2500 ng/mL/day at the end of the step 4. In parallel, AFP was detected at the end of step 3 (39 000 ng /mL/day), but still increase in step 4 (87 000 ng/mL/day), illustrating an immature pattern at the end of our protocol (Fig. 1K).

To benchmark the metabolomic analysis, we measured the level of glucose, lactate and glutamine at the end of each step in the culture medium. We found that glutamine was consumed in the step 1, 2 and 3, whereas it was produced in step 4 (Fig. 1L). Glucose was consumed in each step, leading to consumption of 0.8

mmol/L/day (Fig. 1M). The lactate production was equal to glucose consumption in step 1 (closed to 0,8mmol/L/day) leading to glucose lactate ratio closed to 1 (Fig. 1N). However, in step 2, 3 and 4, we found higher productions of lactate when compared to glucose consuption. The highest levels of lactate were measured in step 4, with production equal to 1.4 mmol/L/day.

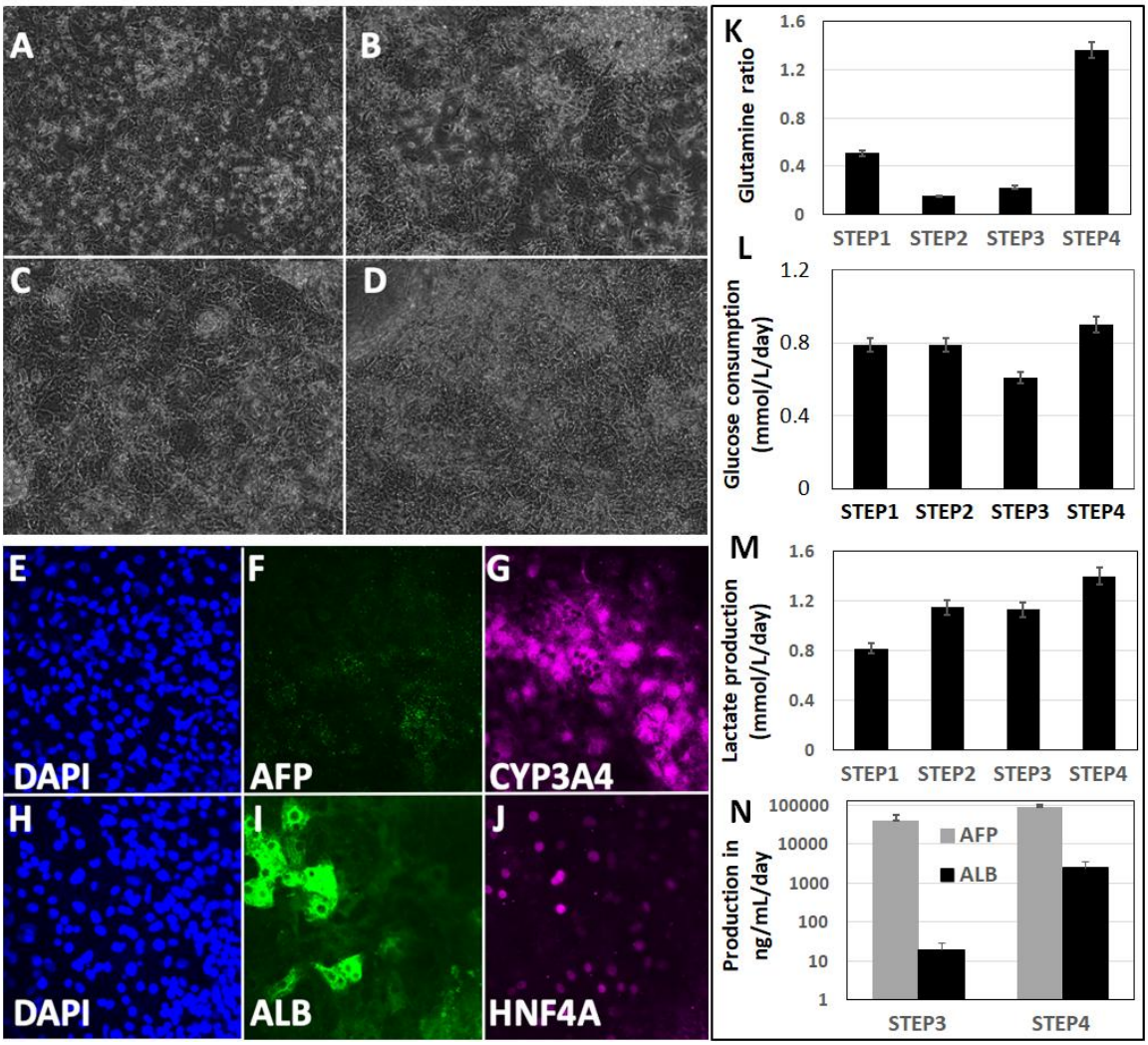


**Fig. 1.** (A-D) Cell morphologies at the end of step 1 to 4; (E-J) Immunostaining at the end of step 4 and (K-N) Basal cell metabolism during the differentiation (ALB: albumin and AFP: alphafetoprotein).

### 3.2. Metabolomic multivariate statistics

The metabolomic analysis lead to identify 111 different compounds in the culture media samples (supplementary file 1). We performed a multivariate analysis on the metabolomic data to identify the specific signatures of each differentiation step. As the culture medium are not the same in the different step, especially in step 4, we performed a normalisation for each compound (using the level of each compound in the basal culture media, the basal media are the control media without cell exposure, supplementary file 1). The overall analysis by PCA could not contribute to separate the step 2 and 3, that were very closed to each other as shown in Fig. 2A. As a result, an additional OPLS-DA contributes to separate the four differentiation steps as shown in Fig. 2B.

The heatmap of the top 40 significant metabolites used to discriminate each step is given in Fig. 2C. Among them, the step 1 was characterised by the levels of aspartic acid, fructose, 3 phosphoglycerate, glutamic acid, elaidic acid. Overall, step 2 and 3 appeared very similar as far as most of metabolites were common in both steps. Nevertheless, the direct comparison between steps 2 and 3, using OPLS-DA treatment, contributes to extract specific signatures in both steps (Fig. S1, supplementary file 2). The step 2 metabolites reveal the importance of aspartic acid, glutamic acid, lactic acid, O-phosphocolamine and citric acid in the discrimination (VIP scores above 1.6). The step 3 was characterised by the level of glucose, galacturonic acid, arabinose, glycerol, alpha ketoglutaric acid and fumaric acid.

The urea, glutamine, methionine sulfoxide, pyroglutamic and pantothenic acid were among the metabolites illustrating the step 4 (Fig. 2C). Finally, the most important metabolites that could be illustrated as potential biomarkers between the steps 1 and 4 are illustrated by the VIP plot in Fig. S2 (supplementary file 2). It included sorbitol, 3-phosphoglycerate, pyroglutamate, fructose, glucose 6 phosphate and glycerol among the top 10 ones (VIP scores above 1.3).

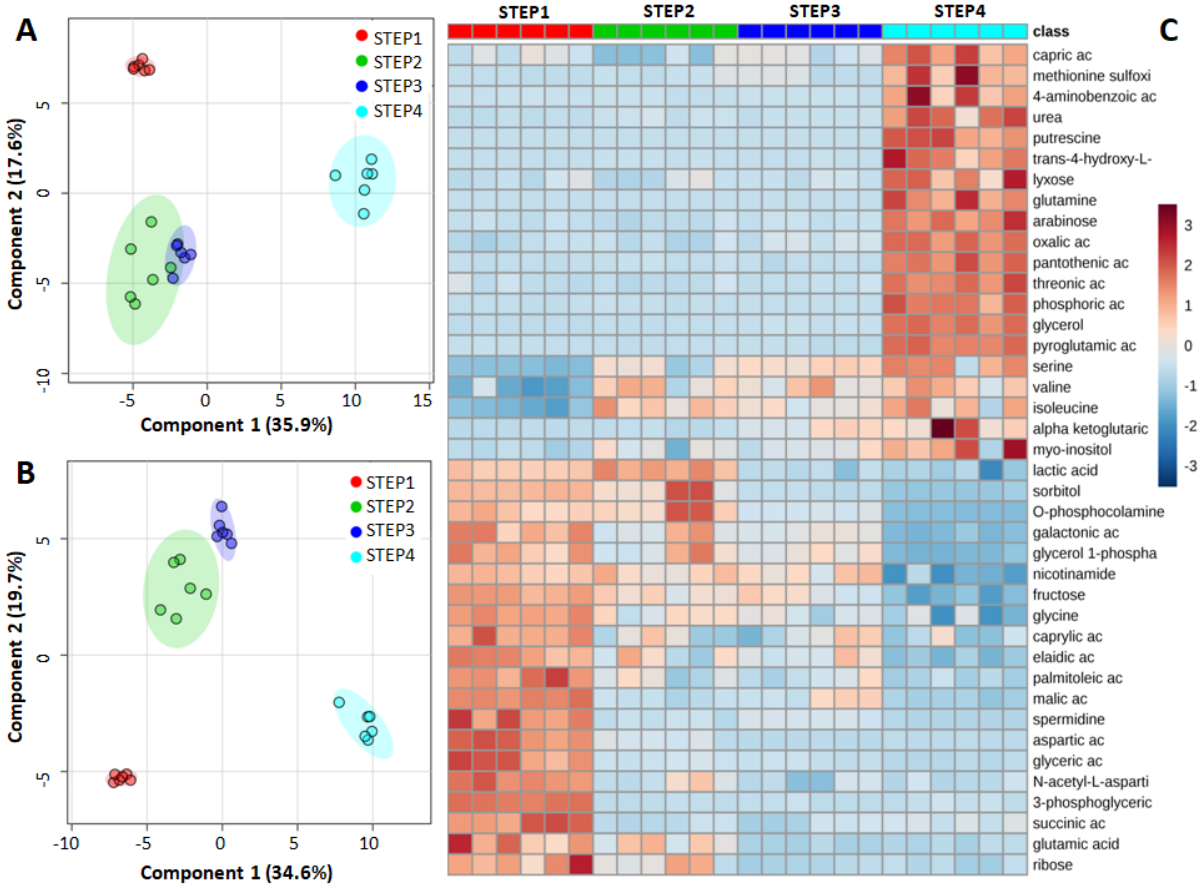


**Fig. 2.** (A) PCA and (B) PLS-DA scores plot discriminating the 4 steps of differentiation, and (C) heatmap of the top 40 metabolites identified by PLS-DA analysis.

### 3.3. Step by step metabolomics signature

In order to identify the metabolomic signature of each differentiation step, we refined the analysis regarding each step compared to basal medium. We focused particularly on the step 1 and 4 of differentiation as a starting and final point, respectively.

At the end of step 1, 61 metabolites were differentially expressed between the basal culture medium and the cell culture medium (*P* value < 0.01, supplementary file 3). The heatmap of top 50 metabolites is presented in Fig. 3A (*P* value < $5x10^{-4}$). In particular, we monitored a decrease of glucose, glutamine and serine levels illustrating a cellular consumption, whereas lactic acid, glutamic acid and glycine increased. We also detected the production of TCA substrates (citric, succinic, malic, fumaric and alpha-ketoglutaric acids) and substrates related to the carbohydrates and pentose phosphate pathway metabolisms (3-phosphoglyceric acid, sorbitol, ribose, xylitol, xylulose and gluconoic acid). Changes in lipid metabolism was illustrated by the degradation of linoleic and heptadecanoic acids (two fatty acids) and the production of hexanoic, lauric , elaidic, azelaic, palmitoleic and phosphoglyceric acids, glycerol-1-phosphate and cholesterol (thus illustrating an oxidation reaction, e.g., cholesterol biosynthesis from fatty acids such as linoleic acids, or pyruvate). Concerning amino acids, the levels of alanine, histidine and proline were increased, while most other amino acids such as cystine, tryptophan, threonine, methionine, tyrosine, lysine, valine, and isoleucine decreased (*n.b.* alanine can be produced either from pyruvate at the end of the glycolysis or from branched chain amino acids such as valine, isoleucine). Finally, the end of step 1 was

characterized by production of xanthine, hypoxanthine and uracil (three compounds resulting from the deamination of guamine, adenine and cytosine) and high levels of O-Phosphocolamine and spermidine. Using the 61 metabolites for pathway analysis with MetaboAnalyst software, we found that ammonia related pathway, spermidine, Warburg effect and aspartic acid metabolisms were among the most modulated pathways as shown in Fig. 4A (completed pathway list is provided in supplementary file 4).

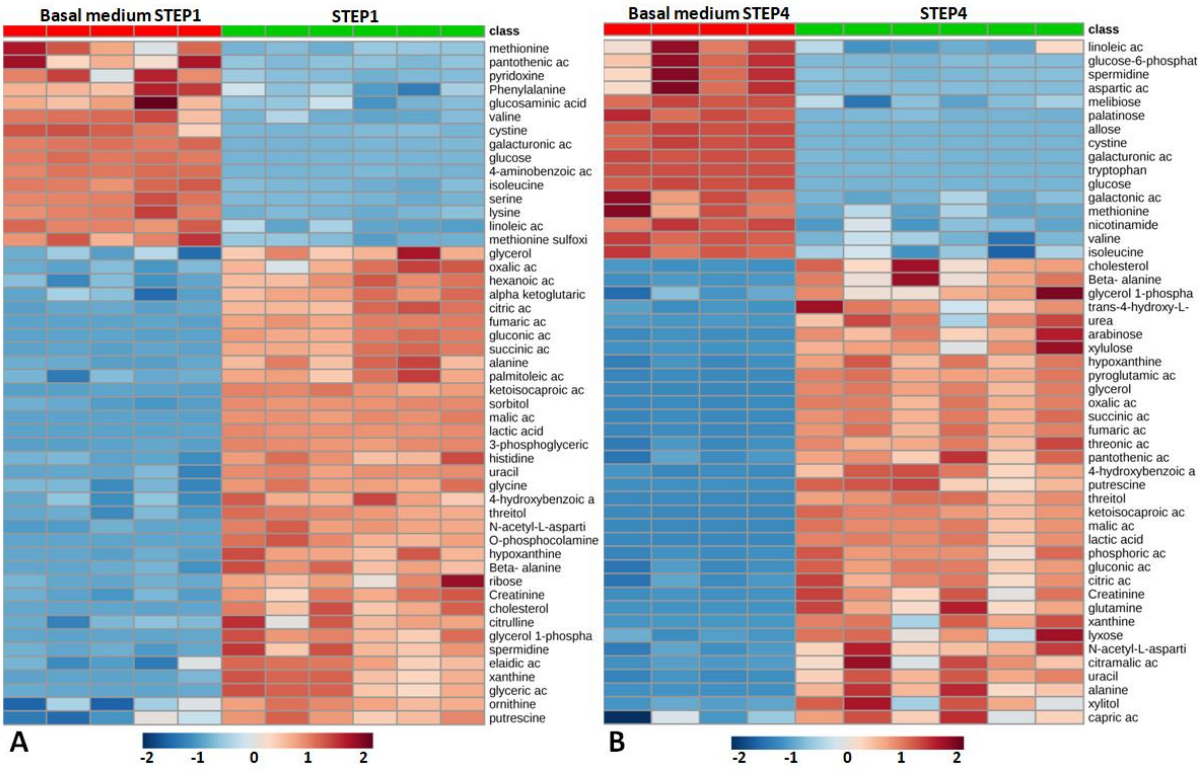


**Fig. 3.** Heatmap of top 50 metabolites modulated in step 1(A) and step 4 (B) of differentiation (in comparison with basal culture medium).

After step 2 and step 3, we detected that 50 metabolites were differentially expressed between the basal culture medium and the cell culture medium (*P* value < 0.01, supplementary file 3). Pathway analysis with 50 metabolites differentially expressed in step 2 revealed the modulation of ammonia recycling pathway, beta-

alanine and aspartate metabolism, TCA cycle and malate-aspartate shuttle (Fig. S3, supplementary file 2). At the end of step 3, ammonia recycling pathway, TCA cycle, malate-aspartate shuttle and mitochondrial electron transport chain were highlighted by MetaboAnalyst analysis (Fig. S3, supplementary file 2).

Finally, at the end of the step 4, we detected that 54 metabolites were differentially expressed between the basal culture medium and the cell culture medium (*P* value < 0.01, supplementary file 3). Refined analysis over the first 50 ones (*P* value < 0.006) showed that 34 metabolites displayed higher levels after cell culture when compared to basal medium (heatmap in Fig. 3B). The last step of differentiation was characterized by high consumption of glucose and lactate production. In addition, consumption of galacturonic and galactonic acids, and glucose-6-phosphate were identified, whereas the levels of several other carbohydrates increased (xylitol, arabinose, lyxose, gluconic acid and xylulose). Urea cycle and polyamine pathway were modulated by enhanced production of glutamine, putrescine, creatinine and urea, and consumption of glutamic acid, spermidine and aspartic acid. We also detected high levels of TCA substrates (citric, succinic, malic and fumaric acids) and decreased concentrations of many amino acids (methionine, cystine, tryptophan, histidine, lysine, valine and isoleucine). Oxidative stress related compounds such as pyroglutamate and methionine sulfoxide were significantly increased and lipid metabolism was illustrated by high levels of glycerol and cholesterol. The pathway analysis with MetaboAnalyst revealed that urea cycle, Warburg effect and aspartic acid related pathways were also modulated as in step 1. Pathways related to gluconeogenesis, mitochondrial chain transport and spermidine

and spermine biosynthesis appeared also as specific targets (Fig. 4B and supplementary file 4).

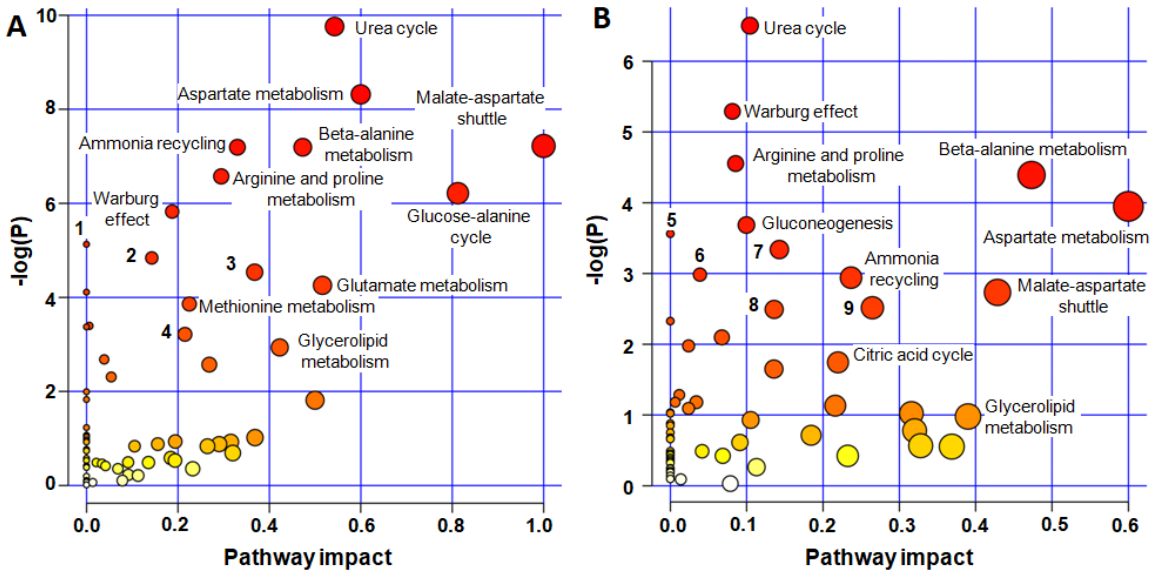


Fig. 4. Metabolic pathways significantly modulated during step 1(A) and step 4 (B) of differentiation (pathways with high pathway impact and/or high P value are labeled). The analysis was performed by MetaboAnalyst software using metabolites with a P value below 0.01. (1) alanine metabolism, (2) spermidine and spermine biosynthesis, (3) glycine and serine metabolism, (4) gluconeogenesis, (5) galactose metabolism, (6) mitochondrial electron transport chain, (7) spermidine and spermine biosynthesis, (8) glutamate metabolism and (9) glycerol phosphate shuttle.

### 3.4. Temporal kinetics during the differentiation between step 1 and 4

In order to follow kinetics of the potential biomarkers during the differentiation, we analyzed and compared the temporal evolution of the metabolites in the culture medium including lipids (Fig. 5A), carbohydrates (Fig. 5B), amino acids (Fig. 5C), krebs cycle substrates (Fig. 6A), glutathione and oxidative stress related compounds (Fig. 6B), urea cycle and polyamines compounds (Fig. 6C) and metabolites

associated to vitamin C and B (Fig. S4, supplementary file 2). Supplementary file 3 provides also the fold change of all detected metabolites (111) during the four differentiation steps.

We measured that the levels of spermidine and 3-phosphoglyceric acid were very high at the end of the step 1 when compared to other steps. Furthermore, we monitored a continuous decrease of the levels of ribose, cysteine, O-phosphocolamine, glycerol-1-phosphate, glyceric acid, palmitoleic acid, elaidic acid, lauric acid, azelaic acid, glutamic acid, tryptophan, cystine, methionine between the step 1 and step 4. In addition, sorbitol level was very high in both step 1 and 2 before to decrease in steps 3 and 4. Similarly xylulose and xylitol were produced in step 4, but their levels were lower when compared to step 1 to 3. We also monitored a switch from histidine production in steps 1 to 3 to histidine consumption in step 4.

In parallel, we measured the continuous increased from step 1 to step 4 of glycerol, putrescine, pyroglutamic acid, urea, serine, kynurenine, alpha keto glutaric acid, proline and hydroxyproline. The level of methionine sulfoxide was high in step 4 when compared to the others step. The step 4 was also characterized by high levels of tyrosine, trans-4-hydroxy-L proline, proline, glutamine, phosphoric acid, oxalic acid, threonic acid.

Malic, citric, succinic gluconic and fumaric acids, creatinine, alanine, hypoxanthine, xanthine and uracil were continuously produced during the differentiation. However, a peak of gluconic acid, hypoxanthine, xanthine and citric acid appeared in step 2, whereas a peak of creatinine was monitored in step 3.

Finally, linoleic acid, heptadecanoic acid, isoleucine, leucine, valine, threonine, were continuously and similarly consumed in the culture medium during the 4 steps of differentiation.

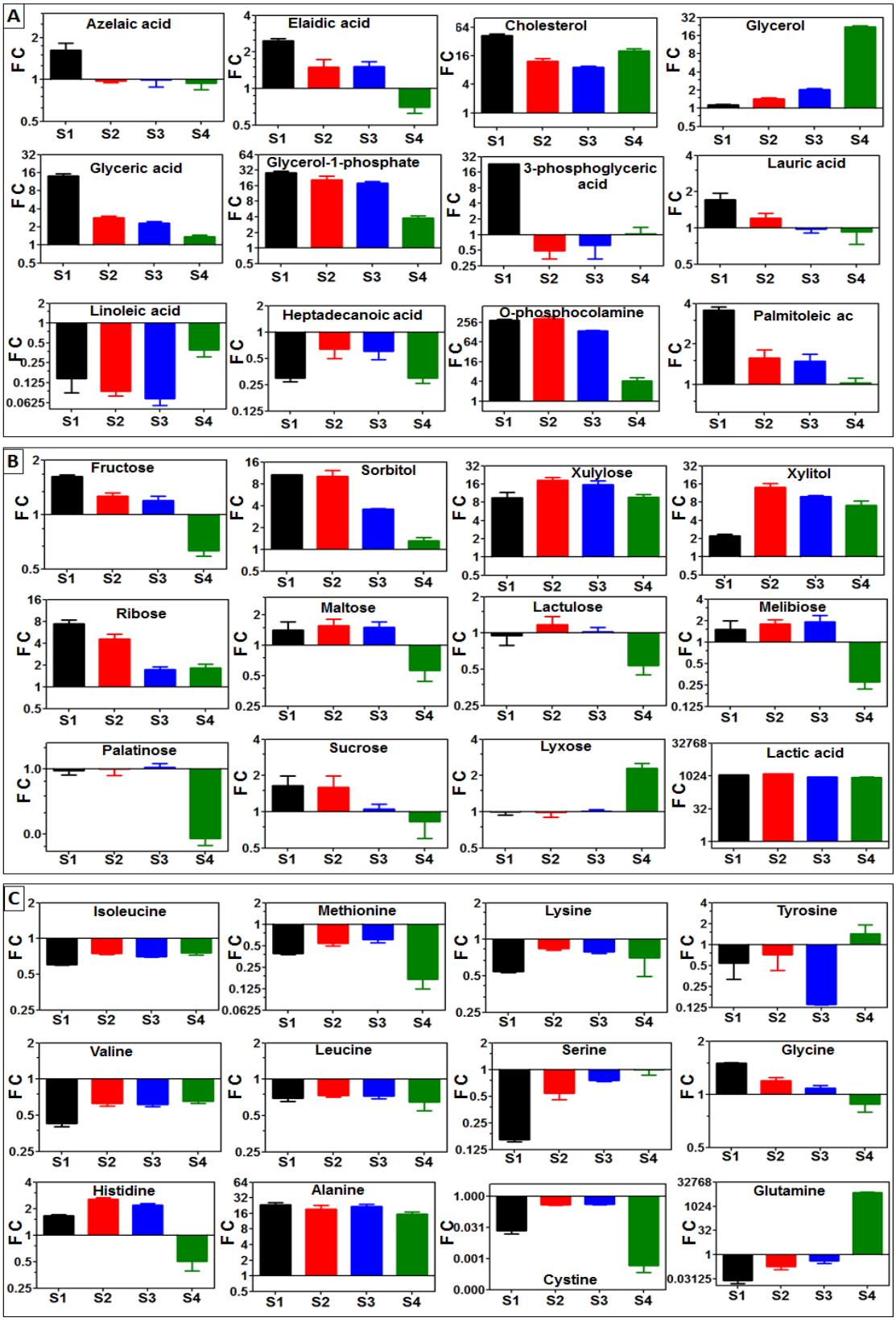

**Fig. 5.** Kinetics of lipid and fatty acids related compounds (A); compounds of the pentose phosphate pathway and various carbohydrates (B) and selected amino acids (C) during the differentiation. FC (fold change) = metabolite level in STEPx / metabolite level in basal medium, FC > 1: metabolite upregulated and FC < 1: metabolites downregulated.

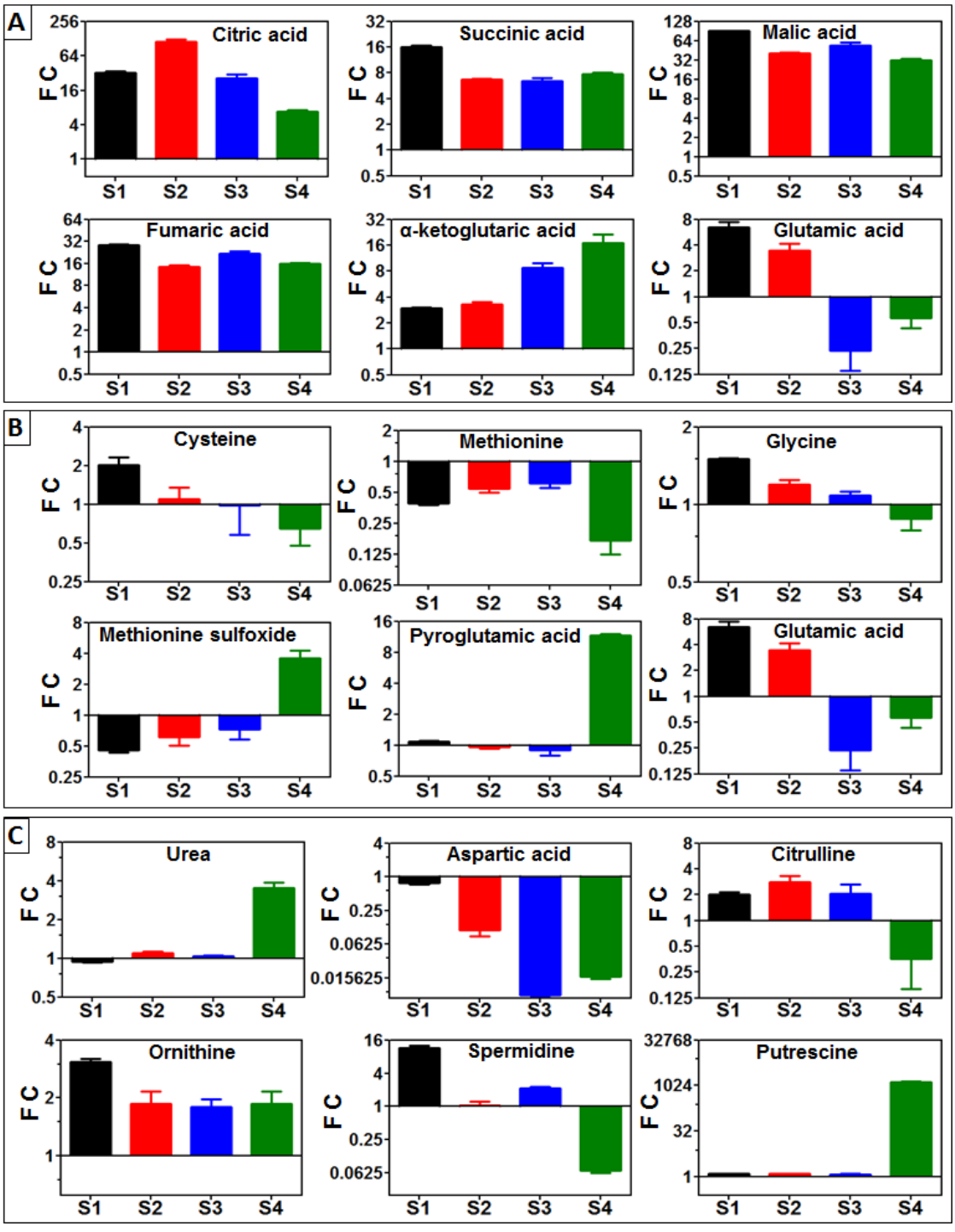

**Fig. 6.** Kinetics of TCA subtrates (A); biomarkers related to glutathione metabolism and oxidative stress (B) and compounds related to urea cycle and polyamine metabolism (C) during the differentiation. FC (fold change) = metabolite level in STEPx / metabolite level in basal medium, FC > 1: metabolite upregulated and FC < 1: metabolites downregulated.

## 4. Discussion

We have performed metabolomic profiling during a step by step differentiation of induced pluripotent stem cells in to hepatocyte like cells. Hepatic phenotype was confirmed at the end of the process by measuring positive cells to glycogen storage, albumin production, and positive immunostaining to CYP3A4. However, mature phenotype was not yet successfully achieved as far as CYP3A4 functionality was not reached. Nevertheless, thanks to the metabolomic profiles we could extract various metabolic switches and patterns as we will discuss now below.

During the step 1, activin A stimulation lead to an activation of several glycolytic pathways as far as we detected glutamine metabolism (glutamine reduction, increase of glutamate), glucose metabolism, sorbitol metabolism and fatty acid degradation pathways (illustrated by linoleic acid degradation and cholesterol formation) and most of the amino acid consumption. The Krebs cycle was also highly activated as illustrated by the high levels of citric, succinic, malic, fumaric and alpha-ketoglutaric acids in the culture medium. Those metabolisms reflected an intense energy demand during the step 1. More particularly the sorbitol pathway is well known to bypass the hexokinase and phosphofructokinase steps in the glycolysis

pathway (Jeffrey et al., 1983). Although we did not identify the specific reason of this activation in our cell, this bypath involves oxidation of molecules of NADPH, thus favoring operation of the pentose phosphate pathway, and is linked to lipid synthesis *via* glycerol formation. This result appeared consistent with our finding of high levels of 3 phosphoglyceric acid, the production of glycerol-1 phosphate and glyceric acid (a glycerol derivative *via* its oxidation), and the intense production of ribose (Mahoney et al., 2018). NADPH is also use for reactive oxygen species detoxification *via* glutathione processing.

In parallel, the glucose/lactate ratio illustrated an aerobic respiration. However, during the step 1, we did not detect specific glutathione metabolism biomarkers (such as high level of pyroglutamate and methionine sulfoxide when compared to step 4, see discussion below) leading to the hypothesis of a glycolysis-based respiration and a yet a weakly mitochondrial oxidative phosphorylation (OXPHOS) respiration. This finding is consistent with literature report in which pluripotent stem cells glucose metabolism is described by an ATP production *via* glycolytic pathway and decoupled from oxygen consumption by the mitochondrial electron transport chain (Shyh-Chang et al., 2013; Zhang et al., 2011). In addition, in this cell stage, folate cycle is activated to maintain the pluripotency of the cells *via* the threonine-glycine catabolism (Jang et al., 2015). This activation is consistent with the glycine, cysteine production and to the high consumptions of serine and threonine in step 1.

During the differentiation of embryonic stem cells, the glycolytic flux and lactate production is dropped leading to a reduction of the pentose phosphate pathway and an increase of the electron transport chain (Shyh-Chang et al., 2013). In

parallel the glycolysis is linked to Krebs cycle as far as pyruvate is transported more efficiently to the mitochondria (Shyh-Chang et al., 2013). Our data appeared in agreement with this finding as far as the level of Ribose, Xylulose, Xylitol, and Sorbitol dropped between the steps 1 and 4. In parallel, the apparition of pyroglutamate and methionine sulfoxide illustrated the detoxification of reactive oxygen species *via* the glutathione metabolism (Lord 2016) and methionine (Dever et al., 2008). The consumption of glutathione precursors in the culture medium, such as glycine, cysteine and glutamic acid also reinforce this hypothesis (in parallel, we observed proline and hydroxy proline production, proline is a degradation compound of glutamate that is required in glutathione synthesis). Thus, the ROS production and their glutathione conjugation for their degradation illustrated a probable higher OXPHOS ATP production in step 4 when compared to step 1.

An important switch monitored during the differentiation is also the activation of the urea cycle at the end of the step 4. The urea is a liver production resulting of the nitrogen waste. Nitrogen can be produced from several reactions of deamination (that mainly occurred in the liver, Berg et al., 2002) such as the glutamate deamination leading to the alpha-ketoglutarate. The urea cycle involved also several compounds such as ornithine, fumaric acid, aspartic acid and citrulline. When the urea was not produced, in steps 1 to 3, we found that the citrulline and ornithine accumulated in the culture medium (especially in step 1). Ornithine could be produced by proline degradation, itself produced by glutamate degradation. Ornithine is degraded in putrescine and then in spermidine in the polyamine pathway, which appeared also consistent with the step 1 high level of spermidine. Then, we observed a high production of putrescine and urea in step 4. In step 4, the spermidine,

ornithine and citrulline levels dropped whereas the putrescine increased when compared to step 1. As putrescine was also reported to be expressed in regenerative liver after HGF stimulation in rat (Fujiwara et al., 1993), our findings could consistent with liver specification after HGF step 3.

Then, several markers reflected the step 4 such as urea, pyroglutamate, putrescine and glycerol. The high levels of oxalic and threonic acids, two end products of the vitamin C (L-ascorbic acid, Linster et al., 2006) metabolism reveal an intense utilization of this compound in step 4. Additional potential markers such as phosphoric and panthotenic acids would request further investigation to understand their signification. Finally, during all the differentiation steps, we observed intense production of xanthine, hypoxanthine and uracil when compared to the basal culture medium levels. That probably illustrated the deamination of guamine, adenine and cytosine in the DNA and ongoing methylation process. Additional sequencing (RNA-seq, Chip-seq and Methyl-seq) would be required to further improve the understanding of this process but also correlated the overall metabolic dataset with intracellular processes.

## Conclusions

We have characterized the metabolomic profiles of the induced pluripotent stem cells during their differentiation into hepatocytes like cells. The OPLS-DA contributes to extract biomarkers in each step illustrating the metabolic signatures of the definitive endoderm, the hepatic specification, the hepatic progenitors and the hepatocyte like cells. We monitored a switch in the respiration mechanism from a

glycolytic respiration in definitive endoderm to an oxidative mitochondrial phosphorylation in hepatocyte like cells. We also observed the activation of the urea cycle in the hepatic like cells. The fatty acid oxidation (linoleic acid and heptadecaneic acid) and lipid formation (palmitoleic, azelaic, elaidic and lauric acids) were higher in definitive endoderm but decreased during the differentiation. Conversely, the glycerol levels in the culture medium continuously increased leading to extract the glycerol as an important biomarker of the step 4.

**Acknowledgment:**

The project was supported by the JSPS Kakenhi 16F16715, the JSPS-CNRS post-doctoral fellowship program of Myriam Lereau-Bernier, P16715, by the UTC foundation *via* the support of Dr Jellali and by the iLite ANR-16-RHUS-0005.

**Conflict of interest**

The authors declare no conflict of interests

**Reference**

Berg, J.M., Tymoczko, J.L., Stryer, L., 2002. The first step in amino acid degradation is the removal of nitrogen, in Biochemistry. 5th edition, New York: W H Freeman; 2002.

Cai, J., Zhao, Y., Liu, Y., Ye, F., Song, Z., Qin, H., Meng, S., Chen, Y., Zhou, R., Song, X., Guo, Y., Ding, M., Deng, H., 2007. Directed differentiation of human embryonic stem cells into functional hepatic cells. Hepatology 45, 1229-1239.

Chen, M., Bisgin, H., Tong, L., Hong, H., Fang, H., Borlak, J., Tong, W., 2014. Toward predictive models for drug-induced liver injury in humans: are we there yet?. Biomark. Med. 8, 201-213.

David, S., Hamilton, J., 2010. Drug-induced liver injury. US. Gastroenterol. Hepatol. Rev. 1, 73–80.

Dever, J., Elfarra, A., 2008. l-Methionine-dl-sulfoxide metabolism and toxicity in freshly isolated mouse hepatocytes: Gender differences and inhibition with aminooxyacetic acid. Drug Metab. Dispos. 36, 2252-2260.

Fiehn, O., 2006. Metabolite profiling in Arabidopsis. Methods Mol. Biol. 323, 439-447.

Fiehn, O., Wohlgemuth, G., Scholz, M., Kind, T., Lee, D.Y., Lu, Y., Moon, S., Nikolau, B., 2008. Quality control for plant metabolomics: reporting MSI-compliant studies. Plant J. 53, 691-704.

Fujiwara, K., Nagoshi, S., Ohno, A., Hirata, K., Ohta, Y., Mochida, S., Tomiya, T., Higashio, K., Kurokawa, K., 1993. Stimulation of liver growth by exogenous human hepatocyte growth factor in normal and partially hepatectomized rats, Hepatology 18, 1443-1449.

Godoy, P., Schmidt-Heck, W., Natarajan, K., Lucendo-Villarin, B., Szkolnicka, D., Asplund, A., Björquist, P., Widera, A., Stöber, R., Campos, G., Hammad, S., Sachinidis, A., Chaudhari, U., Damm, G., Weiss, T.S., Nüssler, A., Synnergren, J., Edlund, K., Küppers-Munther, B., Hay, D.C., Hengstler, J.G., 2015. Gene networks and transcription factor motifs defining the differentiation of stem cells into hepatocyte-like cells. J. Hepatol. 63, 934-942.

Hay, D.C., Fletcher, J., Payne, C., Terrace, J.D., Gallagher, R.C., Snoeys, J., Black, J.R., Wojtacha, D., Samuel, K., Hannoun, Z., Pryde, A., Filippi, C., Currie, I.S., Forbes, S.J., Ross, J.A., Newsome, P.N., Iredale, J.P., 2008. Highly efficient differentiation of hESCs to functional hepatic endoderm requires ActivinA and Wnt3a signalling. Proc. Natl. Acad. Sci. USA. 105, 12301-12306.

Holmgren, G., Sjögren, A.K., Barragan, I., Sabirsh, A., Sartipy, P., Synnergren, J., Björquist, P., Ingelman-Sundberg, M., Andersson, T., Edsbagge, J., 2014. Long-term chronic toxicity testing using human pluripotent stem cell–derived hepatocytes. Drug. Metab. Dispos. 42, 1401-1406.

Jang, H., Yang, J., Lee, E., Cheong, J.H., 2015. Metabolism in embryonic and cancer stemness. Arch. Pharm. Res. 38, 381-388.

Jeffery, J., Jörnvall, H., 1983. Enzyme relationships in a sorbitol pathway that bypasses glycolysis and pentose phosphates in glucose metabolism. Proc. Natl. Acad. Sci. USA. 80, 901-905.

Jellali, R., Gilard, F., Fleury, M.J., Paullier, P., Pandolfi, V., Legallais, C., Leclerc, E., 2018. Metabolomics-on-a-chip approach to study the effects of permethrin (PMT), DDT and their mixture on rat hepatocytes. J. Appl. Toxicol. 38, 1121-1134.

Kuna, L., Bozic, I., Kizivat, T., Bojanic, K., Mrso, M., Kralj, E., Smolic, R., Wu, G.Y., Smolic, M., 2018. Models of Drug Induced Liver Injury (DILI) – Current Issues and Future Perspectives. Curr. Drug. Metab. 19, 830-838.

Linster, C.L., Van Schaftingen, E., 2007. Vitamin C. Biosynthesis, recycling and degradation in mammals. FEBS J. 274, 1-22.

Lord, R., 2016. Long-term patterns of urinary pyroglutamic acid in healthy humans. Physiol. Rep. 4, e12706.

Mahoney, D.E., Hiebert, J.B., Thimmesch, A., Pierce, J.T., Vacek, J.L., Clancy, R.L., Sauer, A.J., Pierce, J.D., 2018. Understanding D-ribose and mitochondrial function. Adv. Biosci. Clin. Med. 6, 1-5.

Mischak, H., Allmaier, G., Apweiler, R., Attwood, T., Baumann, M., Benigni, A., Bennett, S.E., Bischoff, R., Bongcam-Rudloff, E., Capasso, G., Coon, J.J., D'Haese, P., Dominiczak, A.F., Dakna, M., Dihazi, H., Ehrich, J.H., Fernandez-Llama, P., Fliser, D., Frokiaer, J., Garin, J., Girolami, M., Hancock, W.S., Haubitz, M., Hochstrasser, D., Holman, R.R., Ioannidis, J.P., Jankowski, J., Julian, B.A., Klein, J.B., Kolch, W., Luider, T., Massy, Z., Mattes, W.B., Molina, F., Monsarrat, B., Novak, J., Peter, K., Rossing, P., Sánchez-Carbayo, M., Schanstra, J.P., Semmes, O.J., Spasovski, G., Theodorescu, D., Thongboonkerd, V., Vanholder, R., Veenstra, T.D., Weissinger, E., Yamamoto, T., Vlahou, A., 2010. Recommendations for biomarker identification and qualification in clinical proteomics. Sci. Transl. Med. 25, 46ps42.

Nicholson, J.K., Lindon, J.C., Holmes, E., 1999. 'Metabonomics': understanding the metabolic responses of living systems to pathophysiological stimuli via multivariate statistical analysis of biological NMR spectroscopic data. Xenobiotica 29, 1181-1189.

Rashid, S.T., Corbineau, S., Hannan, N., Marciniak, S.J., Miranda, E., Alexander, G., Huang-Doran, I., Griffin, J., Ahrlund-Richter, L., Skepper, J., Semple, R., Weber, A., Lomas, D.A., Vallier, L., 2010. Modeling inherited metabolic disorders of the liver using human induced pluripotent stem cells. J. Clin. Invest. 120, 3127-3136.

Reuben, A., Koch, D.G., Lee, W.M., and the Acute Liver Failure Study Group, 2014. Drug-Induced Acute Liver Failure: Results of a U.S. Multicenter, Prospective Study. Hepatology 52, 2065-2076.

Safaei, A., Arefi Oskouie, A., Mohebbi, S., Rezaei-Tavirani, M., Mahboubi, M., Peyvandi, M., Okhovatian, F., Zamanian-Azodi, M., 2016. Metabolomic analysis of human cirrhosis, hepatocellular carcinoma, non-alcoholic fatty liver disease and non-alcoholic steatohepatitis diseases. Gastroenterol. Hepatol. Bed. Bench. 9, 158-173.

Shyh-Chang, N, Daley, G., Cantley, L., 2013. Stem cell metabolism in tissue development and aging. Development 140, 2535-2547.

Si-Tayeb, K., Noto, F.K., Nagaoka, M., Li, J., Battle, M.A., Duris, C., North, P.E., Dalton, S., Duncan, S.A., 2010. Highly efficient generation of human hepatocyte-like cells from induced pluripotent stem cells. Hepatology 51, 297-305.

Sistare, F., Mattes, W., LeCluyse, E., 2016. The promise of new technologies to reduce, refine, or replace animal use while reducing risks of drug induced liver injury in pharmaceutical development. ILAR J. 57, 186-211.

Sun, Y.V., Hu, Y.J., 2016. Integrative analysis of multi-omics data for discovery and functional studies of complex hman diseases. Adv. Genet. 93, 147-190.

Takahashi, K., Tanabe, K., Ohnuki, M., Narita, M., Ichisaka, T., Tomoda, K., Yamanaka, S., 2007. Induction of pluripotent stem cells from adult human fibroblasts by defined factors. Cell 131, 861-872.

Touboul, T., Hannan, N.R., Corbineau, S., Martinez, A., Martinet, C., Branchereau, S., Mainot, S., Strick-Marchand, H., Pedersen, R., Di Santo, J., Weber, A., Vallier, L., 2010. Generation of functional hepatocytes from human embryonic stem cells under chemically defined conditions that recapitulate liver development. Hepatology 51, 1754-1765.

Wu, S., Liu, Y., Zhu, L., Han, D., Bodinga, M., Yang, X., 2018. Hepatic metabolomic profiling changes along with postnatal liver maturation in breeder roosters. Biol. Open 7, bio028944.

Wruck, W., Kashofer, K., Rehman, S., Daskalaki, A., Berg, D., Gralka, E., Jozefczuk, J., Drews, K., Pandey, V., Regenbrecht, C., Wierling, C.,Turano, P., Korf, U., Zatloukal, K., Lehrach, H., Westerhoff, W., Adjaye, J., 2015. Multi-omic profiles of human non-alcoholic fatty liver disease tissue highlight heterogenic phenotypes. Sci. Data 2, 150068.

Xia, J., Mandal, R., Sinelnikov, I.V., Broadhurst, D., Wishart, D.S., 2012. MetaboAnalyst 2.0-a comprehensive server for metabolomic data analysis. Nucleic Acids Res. 40, 127-133.

Zhang, J., Khvorostov, I., Hong, J.S., Oktay, Y., Vergnes, L., Nuebel, E., Wahjudi, P.N., Setoguchi, K., Wang, G., Do, A., Jung, H.J., McCaffery, J.M., Kurland, I.J., Reue, K., Lee, W.N., Koehler, C.M., Teitell, M.A., 2011. UCP2 regulates energy metabolism and differentiation potential of human pluripotent stem cells. EMBO J. 30, 4860-4873.